2009 American Control Conference
Hyatt Regency Riverfront, St. Louis, MO, USA
June 10-12, 2009

A new operational space trajectory tracking controller for manipulators by using only position measurements*

Javier Moreno–Valenzuela and Ernesto Orozco–Manríquez

Abstract— **Many robotic tasks are specified in terms of the position and orientation (pose) of the robot end–effector. The operational space is defined by a set of generalized coordinates to describe the end–effector pose. The main contribution of this paper is a new operational space trajectory tracking controller, which does not require any velocity measurement. A rigorous stability analysis based on Lyapunov's direct method is presented. The practical viability of the proposed algorithm is explored through real–time experiments in an horizontal planar direct–drive arm with two degrees–of–freedom.**

I. Introduction

It is natural to specify a robotic task through the position and orientation of the robot end–effector with respect to a fixed reference frame, usually at the base of the robot. The pose denotes both the position and orientation of the robot manipulator end–effector. A natural way of representing the end–effector orientation is through the Euler angles, which is a three parameters minimal representation of the end–effector orientation. In this case, at least locally, a set of generalized coordinates can be used to describe the dynamics of the end–effector pose. This way of representing the pose defines the operational space of a robot manipulator . On the other hand, the term task space refers the case in that the orientation is described by the unit quaternion, i.e., a set of four Euler parameters. See, e.g., [13], [8] and [7], and references therein for formal studies on rigid body pose description.

Robot pose tracking control strategies typically require full state measurements, i.e., position and velocity in the joint/pose space. The position and orientation of the end–effector is usually sensed through the direct kinematics model with joint position measurements. However, velocity measurements are not available and they are replaced by numerical derivatives of the position and orientation measurements. Although numerical differentiation of position is a common practice to solve the problem of unmeasurable velocity, sometimes the closed–loop stability can not be guaranteed. This situation has motivated Lyapunov–based control designs to assure pose motion control by using synthesized velocity feedback from position measurements, see, e.g., [15], [2], [16], and references therein. Until now, only a few solutions for the pose trajectory tracking control of robot manipulators by using only position measurements have been proposed.

On the other hand, the robot literature reports that industrial robots are provided with a primary (inner) joint velocity loop, which works together with a task–based secondary (outer) loop [4], [9], [11], [5]. However, these approaches did not addressed the problem of unmeasurable joint/operational space velocity.

The main objective of this paper is to present a new solution for the pose trajectory tracking control problem based on two industrial motivations:

1) The control structure is based on two loops of feedback.
2) Incorporation of synthesized velocity from position measurements.

In particular, the proposed primary joint velocity controller is implemented following the concept of filtering the joint positions via a stable first order system to obtain a synthetic version of the joint velocity. Using the Lyapunov theory framework and cascade systems stability results [10], a rigorous study of the proposed algorithm in closed–loop with the robot arm model is presented.

The main contribution of this paper is a new solution for the pose trajectory tracking control problem based on two loops of feedback. The proposed algorithm incorporates a synthesized velocity feedback from position measurements. Using Lyapunov's direct method cascade systems stability theory, a rigorous study of the closed–loop system is presented. As second contribution, an experimental study carried out in a two degrees–of–freedom direct–drive robot is presented.

Notation: Throughout this paper the following notation will be adopted. $\|\boldsymbol{x}\| = \sqrt{\boldsymbol{x}^T\boldsymbol{x}}$ stands for the norm of vector $\boldsymbol{x} \in \mathbb{R}^n$. $\tanh(\boldsymbol{x}) = [\tanh(x_1) \ \cdots \ \tanh(x_n)]^T$. $\lambda_{min}\{A(\boldsymbol{x})\}$ and $\lambda_{Max}\{A(\boldsymbol{x})\}$ denote the minimum and maximum eigenvalues of a symmetric positive definite matrix $A(\boldsymbol{x}) \in \mathbb{R}^{n\times n}$ for all $\boldsymbol{x} \in \mathbb{R}^n$, respectively. $\|B(\boldsymbol{x})\| = \sqrt{\lambda_{Max}\{B(\boldsymbol{x})^T B(\boldsymbol{x})\}}$ stands for the induced norm of a matrix $B(\boldsymbol{x}) \in \mathbb{R}^{m\times n}$ for all $\boldsymbol{x} \in \mathbb{R}^n$.

II. Robot modeling and control goal

A. Robot dynamics

The dynamics in joint space of a serial–chain n-link robot manipulator considering the presence of friction at the robot joints can be written as [13]

$$M(\boldsymbol{q})\ddot{\boldsymbol{q}} + C(\boldsymbol{q},\dot{\boldsymbol{q}})\dot{\boldsymbol{q}} + \boldsymbol{g}(\boldsymbol{q}) + F_v\dot{\boldsymbol{q}} + \boldsymbol{f}_{Cl}(\dot{\boldsymbol{q}}) = \boldsymbol{\tau} \qquad (1)$$

where $\boldsymbol{q}$ is the $n \times 1$ vector of joint displacements, $\dot{\boldsymbol{q}}$ is the $n \times 1$ vector of joint velocities, $\boldsymbol{\tau}$ is the $n \times 1$ vector of applied torque inputs, $M(\boldsymbol{q})$ is the $n \times n$ symmetric positive definite manipulator inertia matrix, $C(\boldsymbol{q},\dot{\boldsymbol{q}})\dot{\boldsymbol{q}}$ is the $n \times 1$

*This work is partially supported by SNI and SIP-IPN, Mexico.

The authors are with CITEDI-IPN, Av. del Parque 131O, Mesa de Otay, Tijuana, Baja California, C.P. 22510, Mexico, email: moreno@citedi.mx

vector of centripetal and Coriolis torques, $\boldsymbol{g}(\boldsymbol{q})$ is the $n \times 1$ vector of gravitational torques, F_v is a $n \times n$ diagonal positive definite matrix which contains the viscous friction coefficients of each joint, and $\boldsymbol{f}_{Cl}(\dot{\boldsymbol{q}})$ is a continuous and uniformly bounded function, which approaches the behavior of the Coulomb friction.

Assuming that $C(\boldsymbol{q}, \dot{\boldsymbol{q}})$ is expressed in terms of the Christoffel symbols, the following properties on the matrices $M(\boldsymbol{q})$ and $C(\boldsymbol{q}, \dot{\boldsymbol{q}})$ are satisfied [13], [3]:

Property 1. The matrix $C(\boldsymbol{q}, \dot{\boldsymbol{q}})$ and the time derivative of the inertia matrix $\dot{M}(\boldsymbol{q})$ satisfy

$$\boldsymbol{x}^T \left[\frac{1}{2}\dot{M}(\boldsymbol{q}) - C(\boldsymbol{q}, \dot{\boldsymbol{q}}) \right] \boldsymbol{x} = 0 \quad \forall\ \boldsymbol{x}, \boldsymbol{q}, \dot{\boldsymbol{q}} \in \mathbb{R}^n. \tag{2}$$

$$\dot{M}(\boldsymbol{q}) = C(\boldsymbol{q}, \dot{\boldsymbol{q}}) + C^T(\boldsymbol{q}, \dot{\boldsymbol{q}}) \quad \forall\ \boldsymbol{q}, \dot{\boldsymbol{q}} \in \mathbb{R}^n. \tag{3}$$

◇◇◇

Property 2. For all $\boldsymbol{x}$, $\boldsymbol{y}$ and $\boldsymbol{q} \in \mathbb{R}^n$, the inertia matrix $M(\boldsymbol{q})$ is bounded in the sense

$$|\boldsymbol{x}^T M(\boldsymbol{q}) \boldsymbol{y}| \leq \lambda_{Max}\{M(\boldsymbol{q})\} \|\boldsymbol{x}\| \|\boldsymbol{y}\|, \tag{4}$$

$$\lambda_{min}\{M(\boldsymbol{q})\} \boldsymbol{x}^T M(\boldsymbol{q}) \boldsymbol{x} \leq \lambda_{Max}\{M(\boldsymbol{q})\}. \tag{5}$$

◇◇◇

Property 3. For all $\boldsymbol{x}, \boldsymbol{y}, \boldsymbol{z} \in \mathbb{R}^n$ we have that matrix $C(\boldsymbol{x}, \boldsymbol{y})$ satisfies

$$C(\boldsymbol{x}, \boldsymbol{y})\boldsymbol{z} = C(\boldsymbol{x}, \boldsymbol{z})\boldsymbol{y}. \tag{6}$$

$$\|C(\boldsymbol{x}, \boldsymbol{y})\boldsymbol{z}\| \leq k_C \|\boldsymbol{y}\|\, \|\boldsymbol{z}\|, \tag{7}$$

where k_C is strictly positive constant. ◇◇◇

In addition the following two properties are satisfied by the Coulomb–like friction function $\boldsymbol{f}_{Cl}(\dot{\boldsymbol{q}})$:

Property 4. For all $\boldsymbol{x}$, $\boldsymbol{y} \in \mathbb{R}^n$ the following two inequalities

$$[\boldsymbol{x} - \boldsymbol{y}][\boldsymbol{f}_{Cl}(\boldsymbol{x}) - \boldsymbol{f}_{Cl}(\boldsymbol{y})] \geq 0, \tag{8}$$

$$\|[\boldsymbol{f}_{Cl}(\boldsymbol{x}) - \boldsymbol{f}_{Cl}(\boldsymbol{y})]\| \leq k_f \|\boldsymbol{x} - \boldsymbol{y}\|,\ k_f > 0, \tag{9}$$

are satisfied. ◇◇◇

B. Robot kinematics

Denoting $\boldsymbol{h}(\boldsymbol{q}) : \mathbb{R}^n \rightarrow \mathbb{R}^m$ the direct kinematics map, the position and orientation $\boldsymbol{y} \in \mathbb{R}^m$ of the end–effector is given by

$$\boldsymbol{y} = \boldsymbol{h}(\boldsymbol{q}). \tag{10}$$

In particular, the example with natural physical interpretation is the case when $\boldsymbol{y} \in \mathbb{R}^6$. Specifically,

$$\boldsymbol{y} = \begin{bmatrix} \boldsymbol{p}(\boldsymbol{q}) \\ \boldsymbol{\phi}(\boldsymbol{q}) \end{bmatrix}$$

where $\boldsymbol{p} \in \mathbb{R}^3$ denotes the end–effector position in the three dimensional Cartesian space and $\boldsymbol{\phi} = [\varphi\ \vartheta\ \psi]^T \in \mathbb{R}^3$ is the set of three Euler angles which describes end–effector orientation. Let us notice that the Euler angles can be extracted from a given rotation matrix R describing the orientation of the end–effector frame by using the closed–loop inversion formula [13], [1].

The time derivative of the direct kinematic model (10) yields the differential kinematic model

$$\dot{\boldsymbol{y}} = \frac{d}{dt}\boldsymbol{h}(\boldsymbol{q}) = \frac{\partial \boldsymbol{h}}{\partial \boldsymbol{q}}\dot{\boldsymbol{q}} = J(\boldsymbol{q})\dot{\boldsymbol{q}} \tag{11}$$

where $J(\boldsymbol{q})$ is the so–called analytical Jacobian matrix [13], [3]. The robot Jacobian describes a map from velocities in joint space to velocities in operational space. The Jacobian right pseudo inverse [3], is given by

$$J(\boldsymbol{q})^\dagger = J(\boldsymbol{q})^T \left[J(\boldsymbol{q}) J(\boldsymbol{q})^T \right]^{-1},$$

assuming that $J(\boldsymbol{q})J(\boldsymbol{q})^T$ is nonsingular.

Assumption 1. *The analytical Jacobian $J(\boldsymbol{q})$ is assumed of full–rank (rank=m) and bounded by $k_J > 0$, i.e.*

$$\|J(\boldsymbol{q})\| \leq k_J \quad \forall\ \boldsymbol{q} \in \mathbb{R}^n. \tag{12}$$

At the same time, it is also assumed that

$$\|J(\boldsymbol{q})^\dagger\| \leq k_J^\dagger \quad \forall\ \boldsymbol{q} \in \mathbb{R}^n, \tag{13}$$

with $k_J^\dagger > 0$.

◇◇◇

In this paper the notation

$$\dot{J}(\boldsymbol{q}, \dot{\boldsymbol{q}})^\dagger = \frac{d}{dt}\left[J(\boldsymbol{q})^\dagger \right]$$

stands for the time derivative of the Jacobian right pseudo–inverse, which satisfies the following assumptions.

Assumption 2. *The map expressed by the time derivative of the Jacobian right pseudo–inverse satisfies the following relation*

$$\dot{J}(\boldsymbol{q}, \boldsymbol{x} + \boldsymbol{y})^\dagger = \dot{J}(\boldsymbol{q}, \boldsymbol{x})^\dagger + \dot{J}(\boldsymbol{q}, \boldsymbol{y})^\dagger \tag{14}$$

for all $\boldsymbol{q}, \boldsymbol{x}, \boldsymbol{y} \in \mathbb{R}^n$. ◇◇◇

Assumption 3. *The time derivative of the Jacobian right pseudoinverse satisfies the following bound*

$$\left\| \dot{J}(\boldsymbol{q}, \dot{\boldsymbol{x}})^\dagger \right\| \leq k_{J1} \|\dot{\boldsymbol{x}}\| \tag{15}$$

for all $\boldsymbol{q}, \boldsymbol{x} \in \mathbb{R}^{\mathrm{n}}$. ◇◇◇

In practice, assumptions 1–3 are not valid at singularity points [13], [3]. To hold these assumptions, the actual robot pose trajectory should not pass through singular configurations. The global definition of assumptions 1–3 is made to facilitate the stability analysis.

On the other hand, it is possible to show that a planar two degrees–of–freedom revolute joint robot satisfies assumptions 2 and 3. Therefore, these assumptions resemble properties more than assumptions.

C. Control goal

Once the motion specification is given in terms of the desired trajectory $\boldsymbol{y}_d(t)$ in the operational space, then the motion control objective in operational space is to achieve:

$$\lim_{t \rightarrow \infty} \tilde{\boldsymbol{y}}(t) = \boldsymbol{0}, \tag{16}$$

where $\tilde{\boldsymbol{y}}(t) = \boldsymbol{y}_d(t) - \boldsymbol{y}(t)$ denotes the operational space pose error.

III. A CONTROLLER BASED ON SYNTHETIC JOINT VELOCITY FEEDBACK

A. Synthetic velocity controller: Primary loop

The task of the primary control loop is to compute the proper torques and forces $\boldsymbol{\tau} \in \mathbb{R}^n$ so that the joint velocity $\dot{\boldsymbol{q}}$ achieves asymptotic tracking of a desired velocity command $\boldsymbol{\omega}_d$, i.e., $\lim_{t\to\infty} \tilde{\boldsymbol{\omega}}(t) = 0$, where

$$\tilde{\boldsymbol{\omega}}(t) = \boldsymbol{\omega}_d(t) - \dot{\boldsymbol{q}}(t) \tag{17}$$

denotes the joint velocity error. In this paper we assume that the desired joint velocity $\boldsymbol{\omega}_d$ is given as function of time $t \in \mathbb{R}^+$ and the actual joint position $\boldsymbol{q} \in \mathbb{R}^n$, i.e., $\boldsymbol{\omega}_d(t, \boldsymbol{q})$. Therefore, from the joint velocity error definition (17) we can write

$$\dot{\boldsymbol{q}}(t) = \boldsymbol{\omega}_d(t, \boldsymbol{q}(t)) - \tilde{\boldsymbol{\omega}}(t), \tag{18}$$

which is interpreted as the dynamics of the joint position $\boldsymbol{q}(t)$, where the signal $\tilde{\boldsymbol{\omega}}(t)$ is acting as disturbance. By assuring the exponential vanishing of $\tilde{\boldsymbol{\omega}}(t)$ and defining in proper way the desired joint velocity $\boldsymbol{\omega}_d$, the operational motion control objective (16) can be guaranteed. This will be shown in the discussion of the secondary loop. The first step is to show the exponential convergence of $\tilde{\boldsymbol{\omega}}(t)$.

The proposed joint velocity controller is written as follows:

$$\begin{aligned} \boldsymbol{\tau} &= M(\boldsymbol{q})\dot{\boldsymbol{\omega}}_d^\star + C(\boldsymbol{q}, \boldsymbol{\omega}_d)\boldsymbol{\omega}_d + \boldsymbol{g}(\boldsymbol{q}) \\ &\quad + K_v \tanh(\dot{\boldsymbol{\xi}}) + F_v\boldsymbol{\omega}_d + \boldsymbol{f}_{Cl}(\boldsymbol{\omega}_d) \qquad (19) \\ \dot{\boldsymbol{\xi}} &= \boldsymbol{\omega}_d - \boldsymbol{\vartheta} \qquad (20) \end{aligned}$$

where K_v is a $n \times n$ diagonal positive–definite matrix, $\boldsymbol{\vartheta} \in \mathbb{R}^n$ is the output of a first order filter, the desired joint velocity $\boldsymbol{\omega}_d$ is the output of the secondary, and $\dot{\boldsymbol{\omega}}_d^\star$ is a signal called precompensated acceleration, which only depends on time $t \in \mathbb{R}^+$ and the joint position $\boldsymbol{q} \in \mathbb{R}^n$. The signals $\boldsymbol{\omega}_d$ and $\dot{\boldsymbol{\omega}}_d^\star$ will be defined later. For the analysis that is coming, the following assumptions on $\boldsymbol{\omega}_d$ and $\dot{\boldsymbol{\omega}}_d^\star$ will be important.

Assumption 4: *The signals $\boldsymbol{\omega}_d$ and $\dot{\boldsymbol{\omega}}_d^\star$ satisfy:*

1) *The desired joint velocity $\boldsymbol{\omega}_d(t, \boldsymbol{q})$ is bounded for all $t \geq 0$ and $\boldsymbol{q} \in \mathbb{R}^n$, i.e.,*

$$\|\boldsymbol{\omega}_d(t, \boldsymbol{q})\| \leq \|\boldsymbol{\omega}_d\|_M \ \forall\ t \geq 0 \text{ and } \boldsymbol{q} \in \mathbb{R}^n, \tag{21}$$

with $\|\boldsymbol{\omega}_d\|_M$ a strictly positive constant.

2) *The difference between the desired acceleration $\dot{\boldsymbol{\omega}}_d$ and the signal $\dot{\boldsymbol{\omega}}_d^\star$ can be expressed as a function of time $t \in \mathbb{R}^+$, the joint position $\boldsymbol{q} \in \mathbb{R}^n$ and the velocity error $\tilde{\boldsymbol{\omega}} \in \mathbb{R}^n$, i.e.,*

$$\dot{\boldsymbol{\omega}}_d - \dot{\boldsymbol{\omega}}_d^\star = \boldsymbol{\eta}(t, \boldsymbol{q}, \tilde{\boldsymbol{\omega}}). \tag{22}$$

3) *The signal $\boldsymbol{\eta}(t, \boldsymbol{q}, \tilde{\boldsymbol{\omega}})$ can be upper bounded linearly by the velocity error $\tilde{\boldsymbol{\omega}}$, that is,*

$$\|\dot{\boldsymbol{\omega}}_d - \dot{\boldsymbol{\omega}}_d^\star\| = \|\boldsymbol{\eta}(t, \boldsymbol{q}, \tilde{\boldsymbol{\omega}})\| \leq k\|\tilde{\boldsymbol{\omega}}\|, \tag{23}$$

where k is a strictly positive constant.

$\diamond\diamond\diamond$

We will show that a proper definition of $\dot{\boldsymbol{\omega}}_d^\star$ to satisfy (22)–(23) is possible.

The signal $\boldsymbol{\vartheta}$ involved in the joint velocity controller (19)–(20) is obtained from the following first order filter

$$\begin{aligned} \dot{\boldsymbol{x}} &= \tanh(\boldsymbol{\omega}_d - \boldsymbol{\vartheta}) - \boldsymbol{\omega}_d, \qquad (24) \\ \boldsymbol{\vartheta} &= \boldsymbol{\omega}_d + A\boldsymbol{x} + A\boldsymbol{q}, \qquad (25) \end{aligned}$$

where $A = \text{diag}\{a_1, \ldots, a_n\}$ is positive definite.

B. Closed–loop system derivation

It is possible to show that the equation

$$\frac{d}{dt}\dot{\boldsymbol{\xi}} = -A\tanh(\dot{\boldsymbol{\xi}}) + A\tilde{\boldsymbol{\omega}} \tag{26}$$

resumes the dynamics of the velocity filter (24)–(25).

On the other hand, substituting equation (19) in the robot equation (1), and using the robot model property (6), we obtain

$$\begin{aligned} &M(\boldsymbol{q})\dot{\tilde{\boldsymbol{\omega}}} + [C(\boldsymbol{q}, \dot{\boldsymbol{q}}) + C(\boldsymbol{q}, \boldsymbol{\omega}_d)]\tilde{\boldsymbol{\omega}} + K_v \tanh(\dot{\boldsymbol{\xi}}) \\ &+F_v\tilde{\boldsymbol{\omega}} + [\boldsymbol{f}_{Cl}(\boldsymbol{\omega}_d) - \boldsymbol{f}_{Cl}(\dot{\boldsymbol{q}})] - M(\boldsymbol{q})\boldsymbol{\eta}(t, \boldsymbol{q}, \tilde{\boldsymbol{\omega}}) = \boldsymbol{0}. \end{aligned} \tag{27}$$

Equations (18), (26) and (27) represent the closed-loop dynamics, that in state variables is given by

$$\Sigma_1 : \frac{d}{dt}\boldsymbol{q} = \boldsymbol{\omega}_d(t, \boldsymbol{q}) - \tilde{\boldsymbol{\omega}}, \tag{28}$$

$$\Sigma_2 : \frac{d}{dt}\begin{bmatrix} \dot{\boldsymbol{\xi}} \\ \tilde{\boldsymbol{\omega}} \end{bmatrix} = \begin{bmatrix} -A\tanh(\dot{\boldsymbol{\xi}}) + A\tilde{\boldsymbol{\omega}} \\ -M(\boldsymbol{q})^{-1}\boldsymbol{\zeta}(t, \boldsymbol{q}, \dot{\boldsymbol{\xi}}, \tilde{\boldsymbol{\omega}}) + \boldsymbol{\eta}(t, \boldsymbol{q}, \tilde{\boldsymbol{\omega}}) \end{bmatrix} \tag{29}$$

where

$$\begin{aligned} \boldsymbol{\zeta}(t, \boldsymbol{q}, \dot{\boldsymbol{\xi}}, \tilde{\boldsymbol{\omega}}) &= [C(\boldsymbol{q}, \boldsymbol{\omega}_d(t, \boldsymbol{q}) - \tilde{\boldsymbol{\omega}}) + C(\boldsymbol{q}, \boldsymbol{\omega}_d(t, \boldsymbol{q}))]\tilde{\boldsymbol{\omega}} \\ &\quad + K_v \tanh(\dot{\boldsymbol{\xi}}) + F_v\tilde{\boldsymbol{\omega}} + [\boldsymbol{f}_{Cl}(\boldsymbol{\omega}_d) - \boldsymbol{f}_{Cl}(\dot{\boldsymbol{q}})], \end{aligned}$$

$\boldsymbol{\omega}_d(t, \boldsymbol{q})$ is the desired velocity provided by the secondary loop, and $\boldsymbol{\eta}(t, \boldsymbol{q}, \tilde{\boldsymbol{\omega}})$ was defined in (22)–(23).

C. Stability analysis

In order to consider systems Σ_1 and Σ_2, as a cascade [10] we must prove that the overall system (28)–(29) is complete that is, that the solutions can be continued for all $t \geq 0$ and do not blow up in finite time. This allows us to consider Σ_2 as a time–varying system, that is, we regard the robot–joint velocity controller system as a time–varying system dependent on the joint position $\boldsymbol{q}(t)$.

1) Completeness of the closed–loop system: To prove that the system (28)–(29) is complete consider the function

$$W(\boldsymbol{q}, \dot{\boldsymbol{\xi}}, \tilde{\boldsymbol{\omega}}) = \frac{1}{2}\tilde{\boldsymbol{\omega}}^T M(\boldsymbol{q})\tilde{\boldsymbol{\omega}} + \frac{1}{2}\dot{\boldsymbol{\xi}}^T K_v A^{-1}\dot{\boldsymbol{\xi}} + \frac{1}{2}\boldsymbol{q}^T\boldsymbol{q},$$

which is a positive definite and radially unbounded function. By virtue of property 1 in equation (2) the time derivative of $W(\boldsymbol{q}, \dot{\boldsymbol{\xi}}, \tilde{\boldsymbol{\omega}})$ along the closed–loop system trajectories (28)–(29) is given by

$$\begin{aligned} &\dot{W}(\boldsymbol{q}, \dot{\boldsymbol{\xi}}, \tilde{\boldsymbol{\omega}}) = -\tilde{\boldsymbol{\omega}}^T C(\boldsymbol{q}, \boldsymbol{\omega}_d(t, \boldsymbol{q}))\tilde{\boldsymbol{\omega}} - \tilde{\boldsymbol{\omega}}^T K_v \tanh(\dot{\boldsymbol{\xi}}) \\ &-\tilde{\boldsymbol{\omega}}^T F_v\tilde{\boldsymbol{\omega}}^T - \tilde{\boldsymbol{\omega}}^T[\boldsymbol{f}_{Cl}(\boldsymbol{\omega}_d) - \boldsymbol{f}_{Cl}(\dot{\boldsymbol{q}})] + \tilde{\boldsymbol{\omega}}^T M(\boldsymbol{q})\boldsymbol{\eta}(t, \boldsymbol{q}, \tilde{\boldsymbol{\omega}}) \\ &-\dot{\boldsymbol{\xi}}^T K_v \tanh(\dot{\boldsymbol{\xi}}) + \dot{\boldsymbol{\xi}} K_v\tilde{\boldsymbol{\omega}} + \boldsymbol{q}^T\boldsymbol{\omega}_d(t, \boldsymbol{q}) - \boldsymbol{q}^T\tilde{\boldsymbol{\omega}}. \end{aligned}$$

Using the robot model properties (4) and (7), the Coulomb–like friction function property (8), properties of the tangent

hyperbolic function, assumptions (21) and (23), it is possible to show that there exist κ_1 and κ_2 large enough strictly positive constants such that the function $\dot{W}(\boldsymbol{q},\dot{\boldsymbol{\xi}},\tilde{\boldsymbol{\omega}})$ attains the inequality $\dot{W}(\boldsymbol{q},\dot{\boldsymbol{\xi}},\tilde{\boldsymbol{\omega}}) \leq \kappa_1 W(\boldsymbol{q},\dot{\boldsymbol{\xi}},\tilde{\boldsymbol{\omega}}) + \kappa_2\sqrt{W(\boldsymbol{q},\dot{\boldsymbol{\xi}},\tilde{\boldsymbol{\omega}})}$. With the transformation $z = \sqrt{W}$ we obtain $\dot{z} \leq \frac{\kappa_1}{2}z + \frac{\kappa_2}{2}$. It follows using the comparison equations method to show that $z(t) \leq e^{\kappa_1 t/2}z(0) + \frac{\kappa_2}{\kappa_1}[e^{\kappa_1 t/2} - 1]$, that is, $W(t)$ is bounded for all t bounded and since $W(t)$ is positive definite we obtain that the solutions $[\boldsymbol{q}(t)^T\ \dot{\boldsymbol{\xi}}(t)^T\ \tilde{\boldsymbol{\omega}}(t)^T]^T$ exist and can be continued for all $t \geq 0$.

2) Proof of exponential stability: We have proven that the solutions of the closed–loop system Σ_1–Σ_2 can be continued for all $t \geq 0$ thus the subsystem (29) can be interpret as a nonlinear and nonautonomous system, being the state space origin an equilibrium point. In order to show the asymptotic stability of the subsystem Σ_2 in equation (29), the following Lyapunov function candidate is proposed

$$V(t,\tilde{\boldsymbol{\omega}},\dot{\boldsymbol{\xi}}) = \frac{1}{2}\tilde{\boldsymbol{\omega}}^T M(\boldsymbol{q})\tilde{\boldsymbol{\omega}}$$
$$+\sum_{i=1}^{n} k_{vi}a_i^{-1}\ln(|\cosh(\dot{\xi}_i)|) - \alpha\tanh(\dot{\boldsymbol{\xi}})^T M(\boldsymbol{q})\tilde{\boldsymbol{\omega}}, \quad (30)$$

where α is a strictly positive constant. It is possible to show that $V(t,\tilde{\boldsymbol{\omega}},\dot{\boldsymbol{\xi}})$ is globally positive definite for

$$\alpha < \frac{\sqrt{\lambda_{min}\{K_v A^{-1}\}\lambda_{min}\{M(\boldsymbol{q})\}}}{\lambda_{Max}\{M(\boldsymbol{q}\}} = \frac{\sqrt{\lambda_{min}\{K_v\}\lambda_{min}\{M(\boldsymbol{q})\}}}{\sqrt{\lambda_{Max}\{A\}}\lambda_{Max}\{M(\boldsymbol{q}\}}. \quad (31)$$

This can be done by invoking the fact

$$\sum_{i=1}^{n} k_{vi}a_i^{-1}\ln(|\cosh(\dot{\xi}_i)|) \geq \frac{1}{2}\tanh(\boldsymbol{\xi})^T K_v A^{-1}\tanh(\boldsymbol{\xi}),$$

and the robot model properties (4)–(5).

The time derivative of $V(t,\tilde{\boldsymbol{\omega}},\dot{\boldsymbol{\xi}})$ along of the closed–loop system trajectories (29) is given by

$$\dot{V}(t,\tilde{\boldsymbol{\omega}},\dot{\boldsymbol{\xi}}) = -\tilde{\boldsymbol{\omega}}^T C(\boldsymbol{q},\boldsymbol{\omega}_d)\tilde{\boldsymbol{\omega}} - \tilde{\boldsymbol{\omega}}^T F_v\tilde{\boldsymbol{\omega}} - \tilde{\boldsymbol{\omega}}^T[\boldsymbol{f}_{Cl}(\boldsymbol{\omega}_d)$$
$$-\boldsymbol{f}_{Cl}(\dot{\boldsymbol{q}})] + \tilde{\boldsymbol{\omega}}^T M(\boldsymbol{q})\boldsymbol{\eta}(t,\boldsymbol{q},\tilde{\boldsymbol{\omega}}) - \tanh(\dot{\boldsymbol{\xi}})^T K_v\tanh(\dot{\boldsymbol{\xi}})$$
$$+\alpha\tanh(\dot{\boldsymbol{\xi}})C(\boldsymbol{q},\boldsymbol{\omega}_d)\tilde{\boldsymbol{\omega}} + \alpha\tanh(\dot{\boldsymbol{\xi}})^T K_v\tanh(\dot{\boldsymbol{\xi}})$$
$$+\alpha\tanh(\dot{\boldsymbol{\xi}})^T F_v\tilde{\boldsymbol{\omega}} + \alpha\tanh(\dot{\boldsymbol{\xi}})^T[\boldsymbol{f}_{Cl}(\boldsymbol{\omega}_d) - \boldsymbol{f}_{Cl}(\dot{\boldsymbol{q}})]$$
$$-\alpha\tanh(\dot{\boldsymbol{\xi}})^T M(\boldsymbol{q})\boldsymbol{\eta}(t,\boldsymbol{q},\tilde{\boldsymbol{\omega}}) - \alpha\tanh(\dot{\boldsymbol{\xi}})^T C(\boldsymbol{q},\dot{\boldsymbol{q}})^T\tilde{\boldsymbol{\omega}}$$
$$+\alpha\tilde{\boldsymbol{\omega}}^T M(\boldsymbol{q})\mathrm{Sech}^2(\dot{\boldsymbol{\xi}})A\tanh(\dot{\boldsymbol{\xi}}) - \alpha\tilde{\boldsymbol{\omega}}^T M(\boldsymbol{q})\mathrm{Sech}^2(\dot{\boldsymbol{\xi}})A\tilde{\boldsymbol{\omega}},$$

where the property 1 in (2)–(3), property 3 in (6), and property $\frac{d}{dt}\tanh(\boldsymbol{x}) = \mathrm{Sech}^2(\boldsymbol{x})\dot{\boldsymbol{x}} = diag\{\mathrm{Sech}^2(x_1),\ldots,\mathrm{Sech}^2(x_n)\}\dot{\boldsymbol{x}}$ were used.

By virtue of properties (4)–(5), (7)–(9), inequalities (21) and (23), the facts $\|\tanh(\boldsymbol{x})\| \leq \|\boldsymbol{x}\|$ and $\|\tanh(\boldsymbol{x})\| \leq \sqrt{n}$ for all $\boldsymbol{x} \in \mathbb{R}^n$, the following upper bound on $\dot{V}(t,\tilde{\boldsymbol{\omega}},\dot{\boldsymbol{\xi}})$ is obtained

$$\dot{V}(t,\tilde{\boldsymbol{\omega}},\dot{\boldsymbol{\xi}}) \leq -\begin{bmatrix}\|\dot{\boldsymbol{\xi}}\| \\ \|\tilde{\boldsymbol{\omega}}\|\end{bmatrix}^T Q \begin{bmatrix}\|\dot{\boldsymbol{\xi}}\| \\ \|\tilde{\boldsymbol{\omega}}\|\end{bmatrix} - \phi(\dot{\boldsymbol{\xi}})\|\tilde{\boldsymbol{\omega}}\|^2$$

where the entries of the matrix Q are

$$\begin{aligned} Q_{11} &= \lambda_{min}\{K_v\} - \alpha\lambda_{Max}\{K_v\} \\ Q_{12} &= -\frac{1}{2}\alpha[\gamma_1 + \lambda_{Max}\{A\}\lambda_{Max}\{M(\boldsymbol{q})\}] \\ Q_{21} &= -\frac{1}{2}\alpha[\gamma_1 + \lambda_{Max}\{A\}\lambda_{Max}\{M(\boldsymbol{q})\}] \\ Q_{22} &= \lambda_{min}\{F_v\}, \end{aligned}$$

and

$$\phi(\dot{\boldsymbol{\xi}}) = \alpha\Big[\lambda_{min}\{M(\boldsymbol{q})\}\lambda_{min}\{\mathrm{Sech}^2(\dot{\boldsymbol{\xi}})\}\lambda_{min}\{A\} - k_C\sqrt{n}\Big] - \gamma_2,$$

with

$$\begin{aligned} \gamma_1 &= 2k_C\|\boldsymbol{\omega}_d\|_M + \lambda_{Max}\{F_v\} + k_f + k\ \lambda_{Max}\{M(\boldsymbol{q})\}, \\ \gamma_2 &= k_C\|\boldsymbol{\omega}\|_M + k\ \lambda_{Max}\{M(\boldsymbol{q})\}. \end{aligned}$$

A sufficient condition for the Lyapunov function $V(t,\tilde{\boldsymbol{\omega}},\dot{\boldsymbol{\xi}})$ be globally positive definite and radially unbounded, and its time derivative $\dot{V}(t,\tilde{\boldsymbol{\omega}},\dot{\boldsymbol{\xi}})$ be negative definite into the set

$$\Omega = \{\tilde{\boldsymbol{\omega}} \in \mathbb{R}^n\} \times \left\{\dot{\boldsymbol{\xi}} \in D\right\}, \quad (32)$$

with $D = \left\{\dot{\boldsymbol{\xi}} \in \mathbb{R}^n : \|\dot{\boldsymbol{\xi}}\| \leq d\right\}$, is given by the inequality

$$\frac{k_C\|\boldsymbol{\omega}_d\|_M + k\ \lambda_{Max}\{M(\boldsymbol{q})\}}{\lambda_{min}\{M(\boldsymbol{q})\}\lambda_{min}\{A\}\mathrm{sech}^2(d) - k_C\sqrt{n}} < \alpha$$
$$< \min\left\{\frac{\sqrt{\lambda_{min}\{K_v\}\lambda_{min}\{M(\boldsymbol{q})\}}}{\sqrt{\lambda_{Max}\{A\}\lambda_{Max}\{M(\boldsymbol{q})\}}}, \right.$$
$$\left.\frac{\lambda_{min}\{K_v\}}{2\lambda_{min}\{K_v\}}, \frac{\sqrt{\lambda_{min}\{K_v\}\lambda_{Max}\{F_v\}}}{\gamma_1 + \lambda_{Max}\{A\}\lambda_{Max}\{M(\boldsymbol{q})\}}\right\}, \quad (33)$$

which requires large enough values for the filter gain A and the control gain K_v. A simple tuning procedure to select the gains A and K_v that satisfy the condition (33) has been developed. The tuning procedure was not included in the paper due to space limitation.

Therefore, all the conditions to prove that the state space origin of the closed–loop system (29) is locally asymptotically stable are satisfied [6]. As result, it is possible to claim that $[\dot{\boldsymbol{\xi}}(t)^T\ \tilde{\boldsymbol{\omega}}(t)^T]^T \to 0$ as $t \to \infty$ for all initial condition $[\dot{\boldsymbol{\xi}}(0)^T\ \tilde{\boldsymbol{\omega}}(0)^T]^T$ starting at the some domain of attraction $R_A \subset \Omega$, where Ω is defined in (32).

D. Operational space trajectory tracking controller: Secondary loop

We have already shown the exponential convergence of the velocity error $\tilde{\boldsymbol{\omega}}(t)$. The second step is to select a appropriate definition of the the desired joint velocity $\boldsymbol{\omega}_d$. Substituting the velocity error definition $\tilde{\boldsymbol{\omega}}$ in (17) into the differential kinematics (11) we obtain

$$\dot{\boldsymbol{y}} = J(\boldsymbol{q})[\boldsymbol{\omega}_d(t,\boldsymbol{q}) - \tilde{\boldsymbol{\omega}}]. \quad (34)$$

Let us notice that the kinematic control concept [12] considers the system (34) as the robot model, with control input

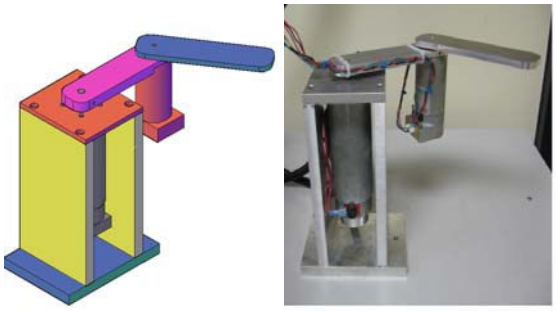

Fig. 1. Experimental robot manipulator actuated by DC motors

$\boldsymbol{\omega}_d(t,\boldsymbol{q})$. Because the analytical robot Jacobian $J(\boldsymbol{q})$ is assumed full–rank, and inspired from the resolved motion rate control philosophy [14], we propose the following control law to generate the desired joint velocity $\boldsymbol{\omega}_d$

$$\boldsymbol{\omega}_d(t,\boldsymbol{q}) = J(\boldsymbol{q})^{\dagger}\left[\dot{\boldsymbol{y}}_d(t) + K\tanh(\tilde{\boldsymbol{y}})\right], \tag{35}$$

with $K \in \mathbb{R}^{m\times m}$ a positive definite matrix and $\tilde{\boldsymbol{y}}(t) = \boldsymbol{y}_d(t) - \boldsymbol{y}(t)$. Note that $\boldsymbol{y} \in \mathbb{R}^m$ can be measured through the direct kinematics map (10). Substituting (35) into (34), the error equation

$$\dot{\tilde{\boldsymbol{y}}} = -K\tanh(\tilde{\boldsymbol{y}}) + J(\boldsymbol{q})\tilde{\boldsymbol{\omega}} \tag{36}$$

is obtained. We have already proven that the synthetic velocity–based controller (19)–(20) achieves exponential tracking of the desired velocity command $\boldsymbol{\omega}_d(t,\boldsymbol{q}(t))$, which implies that $\tilde{\boldsymbol{\omega}}(t)$ vanishes with exponential rate. It is possible to show that the solution $\tilde{\boldsymbol{y}}(t)$ of the undisturbed system $\dot{\tilde{\boldsymbol{y}}} = -K\tanh(\tilde{\boldsymbol{y}})$ is exponentially convergent. Therefore, by invoking the results in [10], and under the assumption that the robot Jacobian $J(\boldsymbol{q})$ is full–rank and bounded, the system (36) has solution $\tilde{\boldsymbol{y}}(t)$ exponentially convergent, this implies that $\lim_{t\to\infty}\tilde{\boldsymbol{y}}(t) = \boldsymbol{0}$. The signal $\dot{\boldsymbol{\omega}}_d^{\star}$ is defined as

$$\dot{\boldsymbol{\omega}}_d^{\star} = \dot{J}(\boldsymbol{q},\boldsymbol{\omega}_d)^{\dagger}\left[\dot{\boldsymbol{y}}_d(t) + K\tanh(\tilde{\boldsymbol{y}})\right] + J(\boldsymbol{q})^{\dagger}\left[\ddot{\boldsymbol{y}}_d(t)\right], \tag{37}$$

By using some direct computations, and the assumption that $\|\dot{\boldsymbol{y}}_d(t)\|$ and $\|\ddot{\boldsymbol{y}}_d(t)\|$ are bounded functions for all $t \geq 0$, it is possible to prove that $\boldsymbol{\omega}_d$ and $\dot{\boldsymbol{\omega}}_d^{\star}$ in (35) and (37), respectively, satisfy the assumption 4 in (21)–(23).

IV. Experimental results

A planar two degrees–of–freedom direct–drive arm has been built at the CITEDI–IPN Research Center. The system is composed by two DC *Pittman* motors operated in current mode with two *Advanced Motion Controls* servo amplifiers. A *Sensoray 626* I/O card is used to read encoder signals with quadrature included and control commands are transferred through the D/A channels. The control system is running in real–time with a 1 kHz sampling rate on a PC over *Windows XP* using *Matlab* with *Simulink* and the *Real–Time Windows Target*.

The DC motors actuators are operated in current mode, then the torque delivered is given by

$$\boldsymbol{\tau} = K\boldsymbol{u}, \tag{38}$$

with $K = diag\{k_1,\ldots,k_n\}$ [Nm/Volt] is a positive definite matrix that contains the motor constants and $\boldsymbol{u} \in \mathbb{R}^n$ is the applied control voltage.

Under the consideration that the actuator torque is given by (38), the proposed controller (19) can be implemented as

$$\boldsymbol{u} = K^{-1}\left[M(\boldsymbol{q})\dot{\boldsymbol{\omega}}_d^{\star} + C(\boldsymbol{q},\boldsymbol{\omega}_d)\boldsymbol{\omega}_d + \boldsymbol{g}(\boldsymbol{q}) + F_v\boldsymbol{\omega}_d + \boldsymbol{f}_{Cl}(\boldsymbol{\omega}_d)\right] + K_v'\tanh(\dot{\boldsymbol{\xi}}), \tag{39}$$

with $K_v' = K^{-1}K_v$. It is noteworthy that the control law (39) can be implemented without knowing the matrix K. This is achieved by noting that the robot model can be written as follows:

$$K^{-1}M(\boldsymbol{q}) = \begin{bmatrix} \theta_1 + 2\theta_2\cos(q_2) & \theta_3 + \theta_2\cos(q_2) \\ \theta_4 + \theta_5\cos(q_2) & \theta_6 \end{bmatrix}, \tag{40}$$

$$K^{-1}C(\boldsymbol{q},\dot{\boldsymbol{q}}) = \begin{bmatrix} -\theta_2\sin(q_2)\dot{q}_2 & -\theta_2\sin(q_2)[\dot{q}_1+\dot{q}_2] \\ \theta_5\sin(q_2)\dot{q}_1 & 0 \end{bmatrix}, \tag{41}$$

$$K^{-1}F_v = diag\{\theta_7,\theta_8\}, \tag{42}$$

$$K^{-1}\boldsymbol{f}_{Cl}(\dot{\boldsymbol{q}}) = \begin{bmatrix} k_1^{-1}f_{Cl1}(\dot{q}_1) = \begin{cases} \theta_9\tanh(50\dot{q}_1) \text{ if } \dot{q}_1 \geq 0, \\ \theta_{10}\tanh(50\dot{q}_1) \text{ if } \dot{q}_1 < 0, \end{cases} \\ k_2^{-1}f_{Cl2}(\dot{q}_2) = \begin{cases} \theta_{11}\tanh(50\dot{q}_2) \text{ if } \dot{q}_2 \geq 0, \\ \theta_{12}\tanh(50\dot{q}_2) \text{ if } \dot{q}_2 < 0, \end{cases} \end{bmatrix}, \tag{43}$$

$$K^{-1}\boldsymbol{g}(\boldsymbol{q}) = 0. \tag{44}$$

It is possible to show that the Coulomb–like function $\boldsymbol{f}_{Cl}(\dot{\boldsymbol{q}})$ in (43) satisfies the property 4 in equations (8)–(9). By using the recursive least squares identification method, we have estimated the coefficients involved in robot model (40)–(44). See Table I.

TABLE I

Estimated parameters

θ_1	0.0480	θ_5	0.0226	θ_9	0.0560
θ_2	0.0038	θ_6	0.0166	θ_{10}	0.0057
θ_3	0.0033	θ_7	0.0073	θ_{11}	0.0611
θ_4	0.0158	θ_8	0.0066	θ_{12}	0.0137

The desired trajectory is given by

$$\boldsymbol{y}_d(t) = \begin{bmatrix} y_{d1c} + r_0\sin(\frac{v_0}{r_0}t) \\ y_{d2c} + r_0\cos(\frac{v_0}{r_0}t) \end{bmatrix} \text{ [m]},$$

with parameters $y_{d1c} = 0.15$ [m], $y_{d2c} = 0$ [m] r_0=0.05 [m] and v_0=0.15 [m/sec]. The robot initial conditions were $\boldsymbol{q}(0) = [42\ 97]^T$ [degrees], which implies that $\tilde{\boldsymbol{y}}(0) = \boldsymbol{0}$.

By using equation (39), we have implemented the joint velocity controller (19)–(20), filter (24)–(25), and operational space controller (35) and (37), with gains $K_v' = diag\{0.4, 0.4\}$ [Volt sec/rad], $A = diag\{1000, 1000\}$ [1/sec], and $K = diag\{7.5, 10.0\}$ [1/sec]. With these control and filter gains, the assumption (33) is satisfied. The initial condition for the filter (24)–(25) was $\boldsymbol{x}(0) = [-0.7303\ \ -1.6901]^T$ [rad], implying that $\boldsymbol{\vartheta}(0) = \boldsymbol{0}$.

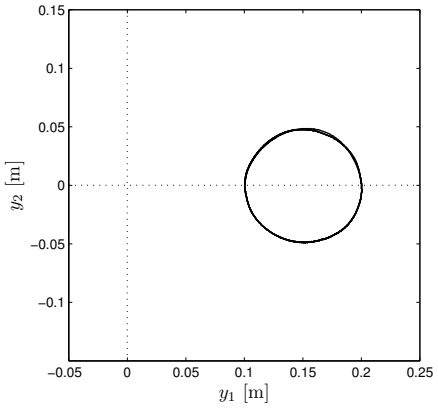

Fig. 2. New controller: Robot path in Cartesian coordinates

The results of the implementation of the new controller (19)–(20), which incorporates the filter (24)–(25), kinematic controller (35) and precompensated acceleration signal (37), is shown in Figure 2, that depicts the Cartesian robot path, Figure 3, which shows the time history of the robot Cartesian position $y_1(t)$ and $y_2(t)$, and Figure 4, that describes the applied control voltages $u_1(t)$ and $u_2(t)$.

Let us notice that high frequency components appeared in the experimental control signals $u_1(t)$ and $u_2(t)$, as seen in Figure 4. The reasons were the 2000 [ppr] encoder resolution of the robot actuators, discrete implementation of the controller and filter, quantization errors, and PWM switching of the servo amplifiers. But in spite of the high frequency contents in the voltage control signal, we did not observe negative effects in the performance of the robot, such as mechanical vibrations.

By using the robot model in (40)–(44), with the estimated parameters in Table I, and taking into account the above–mentioned effects, we have assessed the performance of the new controller with respect to numerical simulations. The results in Figures 3 and 4 indicate that the experimental and simulation results are very similar. In addition, numerical simulation showed that the high frequency contents of the control signals $u_1(t)$ and $u_2(t)$ was owing mainly to the encoder resolution of the robot actuators.

REFERENCES

[1] F. Caccavale, C. Natale, B. Siciliano and L. Villani, "Resolved–Acceleration Control of Robot Manipulators: A Critical Review with Experiments", *Robotica*, Vol. 16, No. 5, pp. 565–573, 1998.

[2] F. Caccavale, C. Natale and L. Villani, "Task–Space Tracking Control Without Velocity Measurements", *Proc. of the 1999 IEEE International Conference on Robotics and Automation*, May 1999, Detroit, MI, pp. 512-517.

[3] C. Canudas de Wit, B. Siciliano, G. Bastin (Eds.), *Theory of Robot Control*, Springer–Verlag, London, 1996.

[4] P. Corke, *The Unimation Puma Servo System*, Report MTM–226, CSIRO Division of Manufacturing Technology, Australia, July, 1994.

[5] R. Kelly and J. Moreno, "Manipulator Motion Control in Operational Space Using Joint Velocity Inner Loops", *Automatica*, Vol. 41, No. 8, pp. 1423-1432, 2005.

[6] H. Khalil, *Nonlinear Systems*, Prentice–Hall, Upper Saddle River, 1996.

[7] O. Khatib, "A Unified Approach to Motion and Force Control of Robot Manipulators: The Operational Space Formulation", *IEEE Journal on Robotics and Automation*, Vol. 3, No. 1, pp. 43-53, 1987.

[8] C. Natale, *Interaction Control of Robot Manipulators: Six Degrees–Of–Freedom Tasks*, Springer, Germany, 2003.

[9] K. Nilsson, *Industrial Robot Programming*, Ph.D. thesis, Lund Institute of Technology, Dept. of Automatic Control, Sweden, 1996.

[10] E. Panteley and A. Loria, "On Global Uniform Asymptotic Stability of Nonlinear Time–Varying Systems in Cascade", *Systems and Control Letters*, Vo. 33, pp. 131–138, 1998.

[11] J. Roy and and L.L Whitcomb, "Adaptive Force Control of Position/Velocity Controlled Robots: Theory and Experiments", *IEEE Trans. on Robotics and Automation*, Vol. 18, No. 2, pp. 121–137, 2002.

[12] B. Siciliano, "Kinematic Control of Redundant Robot Manipulators", *Journal of Intelligent and Robotic Systems*, Vol. 3, pp. 201–212, 1990.

[13] L. Sciavicco and B. Siciliano, *Modelling and Control of Robot Manipulators*, Springer, London, 2000.

[14] D.E. Whitney, "Resolved Motion Rate Control of Manipulators and Human Prostheses", *IEEE Trans. on Man–Machine Systems*, Vol. MMS–10, No. 2, pp. 47–53, 1969.

[15] H. Wong, M.S. de Queiroz and V. Kapila, "Adaptive Tracking Control Using Synthesized Velocity From Attitude Measurements", *Automatica*, Vol. 37, No. 6, pp. 947–953, 2001.

[16] B. Xian, M.S. de Queiroz, D. Dawson and I. Walker, "Task–Space Tracking Control of Robot Manipulators Via Quaternion Feedback", *IEEE Trans. on Robotics and Automation*, Vol. 20, No. 1, pp. 160–167, 2004.

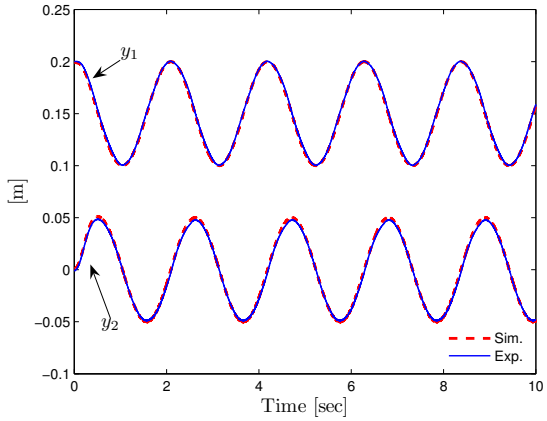

Fig. 3. New controller: Time history of the robot Cartesian position $y_1(t)$ and $y_2(t)$ by experiment and numerical simulation

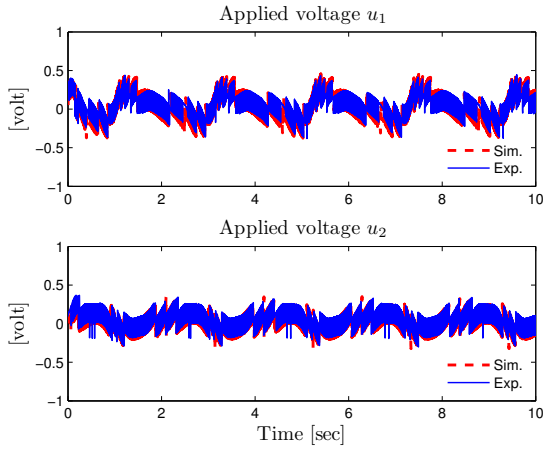

Fig. 4. New controller: Applied voltages $u_1(t)$ and $u_2(t)$ by experiment and numerical simulation